Letters in Applied NanoBioScience
Open-Access Journal (ISSN: 2284-6808)

Article
Volume 14, Issue 1, 2025, 40
https://doi.org/10.33263/LIANBS141.040

Adsorption and Biological Evaluation on the Malachite green dye using CuO-ZnO Nanoparticles

Lubna Afroz [1], Moodgere Habeebulla Moinuddin Khan [1,*], Roopashree B [2], Puneetha J [2], Basavaraja Patel B M [3]

[1] Department of Chemistry, JNN College of Engineering, (VTU) Shivamogga-577204, Karnataka, India
[2] Department of Chemistry, JSS Academy of Technical Education, Bengaluru, Affiliated to Visvesvaraya Technological University, Bangalore - 560 060, Karnataka, India
[3] Department of Chemistry, AMC Engineering College, Bangalore - 560 083, Karnataka, India
* Correspondence: drmk@jnnce.ac.in;

Scopus Author ID 52463848200
Received: 20.03.2023; Accepted: 12.05.2023; Published: 28.09.2024

Abstract: Malachite green dye was removed from an aqueous medium using an inexpensive CuO - ZnO NPs and NCs adsorbent, which is commercially available. Materials were characterized using scanning electron microscopy (SEM) and Fourier transform infrared spectroscopy (FTIR) to analyze the adsorbent. Some variables influencing the dye removal rate include pH, initial dye concentration, adsorbent dose, contact time, and temperature. Within the 180-minute equilibration time, a high removal efficiency of 78% was achieved using a reducing dye with a strength of 94 mg/g, a dosage of 0.8 g, and a pH of 8. The results demonstrated by the cited method supported the adsorbent's effectiveness in removing dye. Because of the efficiency in the dye removal, antimicrobial activity was also performed, showcasing the better synergistic effects of NCs. Furthermore, the antioxidant and antihemolytic activities were studied, and the CuO-ZnO displayed significant prior-mentioned activities. As a result, the synthetic materials showed promising biological efficacies and the ability to remove the color from textile industry wastewater.

Keywords: Co-precipitation technique; adsorption; antimicrobial; antioxidant; antihemolytic activity.

1. Introduction

Organic and inorganic contaminants in water and air can be degraded using the intriguing photocatalysis method. Semiconductor oxides, particularly TiO_2 and ZnO, have been considered the finest products for photocatalytic processes because of their non-toxicity, chemical stability, significant photosensitivity, and relatively low price [1]. Due to their broadband gaps, TiO_2 and ZnO can hardly accumulate a finite potential to withstand a small portion of the UV range of light. As a result, it continues to be challenging to utilize solar energy in photocatalytic degradation effectively. Enhancing the visible light spectrum that ZnO and TiO2 can absorb has been attempted in numerous ways, including transition-metal ion doping, noble metal deposition, interrelated semiconductor systems, etc. ZnO and CuO NPs have grabbed the attention of different metal oxide NPs due to their diverse applications and physiochemical properties. ZnO NPs are used in several industries, such as cosmetics, batteries, glass, ceramics, lubricants, food, plastics, paints, adhesives, etc. CuO NPs are used in electronics and other technologies due to their unique and excellent thermophysical properties.

Various studies have demonstrated the effects of ZnO and CuO NPs on plants, which reveal that potential phytotoxicity depends upon their concentration, shape, size, etc.

Coupled semiconductors made of various sulfide or metal oxides and ZnO, including Fe_2O_3, SnO_2, CdS, TiO_2, CuO, WO_3, and ZnS, have been studied recently [2]. The findings show that coupling various semiconductor oxides may increase the visible light absorption range and decrease the band gap. This leads to an increase in the photocatalytic activity by causing electron-hole pair dissociation during irradiation. When water is degraded into O2 and H2 under the effect of solar light, CuO powder has the potential to trigger this reaction. Xinxin Lu *et al*. [3] originally reported this capability of CuO powder in 2020. CuO demonstrated the highest catalytic activity and stability in this process. The CuO molecule has a 2.0 eV narrow band gap. Thus, under the influence of visible light, electrons at the ground band are easily excited. CuO has a modest catalytic activity due to the ease with which electrons and holes recombine. However, the weak catalytic activity of CuO is due to the simple recombination of holes, and electrons have been synthesized by various methods like sol-gel, thermal, osmosis, etc. Among these, we have chosen the co-precipitation method of metal-based nanoparticles by direct precipitation at low concentration and temperature, which benefits the measurement of trace elements that can be detected at highly efficient and a wide range of analytes of a mass greater than a magnitude of a source of contamination which can be removed by this precipitate matrix for further filtration and internal standard elements which can be handled in one step process. Li *et al*. [4] produced the TiO_2- CuO composite oxides through the combination of CuO with commercial TiO_2(70%) anatase with a minor amount of rutile and a small amount of amorphous phase) to affect the content of the interaction. They discovered that this combination had a methodology that would make the dye brilliant red degrade more instantly when exposed to visible light. Thus, the abovementioned facts compelled us to modify the material's properties by changing the composition, crystalline structure, particle size, morphology, and stability of the final products at a low cost.

As per the literature, adsorption is the most commonly used method for the removal of both organic and inorganic pollutants from industrial wastewater. Adsorption material is available from various sources, such as natural sources such as agricultural and industrial wastes. Dye removal from wastewater using activated carbon is an effective method, but in industrial processes, it was restricted due to its high operational and investment costs. In the adsorption method, various other natural sources are available to remove dyes from industrial wastewater. Among all the methods available for separating pollutants from waste water, adsorption shows a possible method for treating and removing organic pollutants in wastewater treatment. To evaluate and expect to produce less toxic and more degradable NP to minimize the environmental risk in the future. The removal of pollutants in simulated wastewater by nanocomposites was found to be excellent. Still, there is a need for further clarification on the adsorption mechanism of the nano adsorbents for pollutants present in complex industrial wastewater. In the present paper, we reported the properties of CuO (in the oxidation state of +2) prepared via precipitation. The resulting CuO was later doped on zinc oxide (ZnO) for adsorption efficacy by including the first-ever study of biological activity that has been conducted on the use of CuO-ZnO nanoparticle to remove Malachite green dye from water.

2. Materials and Methods

2.1. Resources and instrumentation.

Sources of zinc and copper utilized were Zinc nitrate (Zn (NO3)2.6H2O) (AR 99% Merck) and copper sulfate ($CuSO_4.5H_2O$) (AR 99% Merck). The reducing agent employed was hydrazine hydrate (N2H4.H2O) (AR 99% Merck). Since it has often been used as an indication for the adsorption activities due to its absorption maxima in the visible light range, Malachite green dye (AR 99% Merck) was adopted as the indicator. Distilled water was used to make each solution. X-ray Diffractometer (Rigaku Miniflex 600,5th gen) with Cu-Kα radiation (wavelength 0.154nm), Systronics UV–VIS spectrometer-119 was utilized. The surface morphology of the synthesized compounds was deduced via a Zeiss scanning electron microscope.

2.2. Preparation of adsorbent.

The co-precipitation method was used to create the adsorbent for the CuO -ZnO Nps and NCs combination. Typically, 0.04M Zn (NO_3)2.6H_2O was dissolved in 100mL of water using a magnetic stirrer, and hydrazine hydrate ($N_2H_4.H_2O$) was added. The solution was stirred ferociously for 20 minutes at room temperature to ensure enough Cu^{2+} ions were adsorbed on the surface of zinc nitrate [5]. The mixed solution was stirred with a magnetic stirrer at 60°C and evaporated for 3 hours to obtain the ZnO Nps. To this mixture, 1 g of copper sulfate (CuSO4.5H2O) was stirred for about 60 min. The solution was heated to 80 °C for 3 hrs to obtain crude CuO - ZnO precipitate, as depicted in Figure 1. The precipitate was filtered and cleaned using double distilled water six times to neutralize it. The product was oven-dried at 60 °C for 2 hr.

2.3. Statistical optimization of process parameters.

Factors affecting the adsorption process and adsorption capacity were studied, such as the influence of contact time (A), temperature (B), initial dye concentration (C), adsorbent dosage (D), and initial pH (E) were included in studies. These independent variables were adjusted for adsorption capacity, which is the dependent response variable at fixed orbital shaking at 155 rpm. A design of standard experimental was prepared comprising six factors at two levels (Table 1). Upon analyzing the variance, a general quadratic regression equation was yielded. Surface and contour plots were obtained, indicating graphically the individual as well as interaction effects between parameters on the adsorption capacity [6].

Table 1. The experimental range for individual factors.

Factor	Name	Units	Minimum	Maximum
A	Time	Minute	0	90
B	pH	-	2	14
C	Adsorbent dosage	g/L	0.1	5
D	Concentration	mg/L	10	500
E	Temperature	°C	27	40

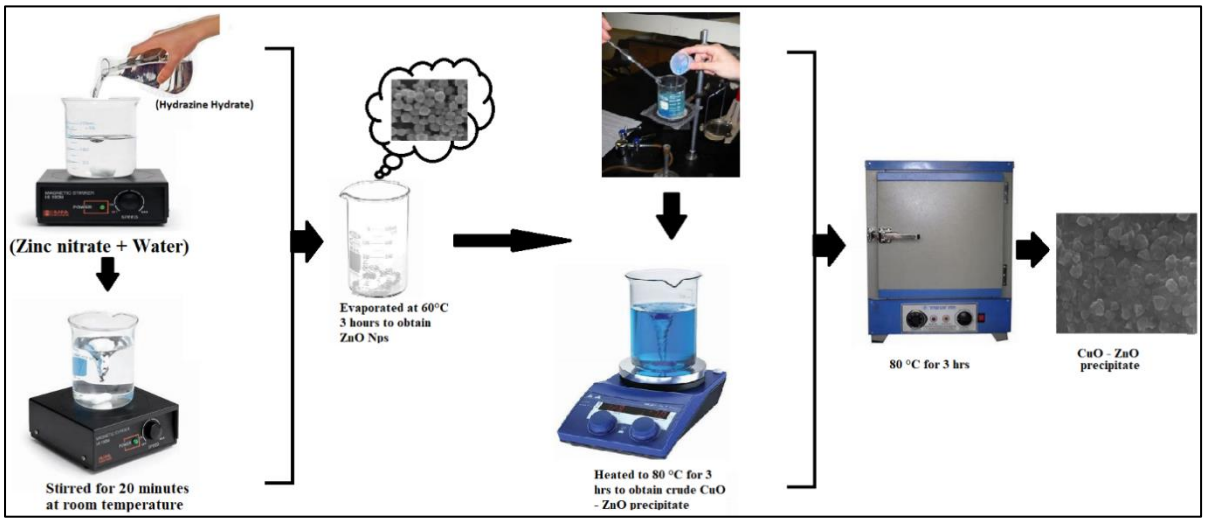

Figure 1. Preparation of adsorbent CuO - ZnO precipitate.

2.4. Antibacterial screening.

Using an agar well-diffusion approach, metal-based NP and NC were tested for their antibacterial effectiveness against four different bacterial species, including *Staphylococcus aureus*, *Escherichia coli*, *Bacillus subtilis*, and *Salmonella Typhi*. A sterile cork borer was used to puncture a 9-mm well in a Muller-Hinton agar plate after adding a 24-year-old Muller-Hinton broth culture of the test bacteria. Chloramphenicol was employed as a standard in two different concentrations (10% DMSO in 100 and 200 g/mL), and control (10% DMSO) was added to designated labeled wells. The plates were allowed to stand for around 30 minutes before being incubated for 24 hours at 37 °C in an upright posture. At this time, more test solution was seen to diffuse, and the zone of inhibition was measured using vernier calipers [7,8].

2.5. Antifungal screening.

Using the Sabouraud dextrose agar diffusion method, metal-based NP and NC were assessed for their antifungal efficacy against the fungus Candida albicans and Aspergillus niger. Wells were made using a cork borer that had been cleaned (9 mm diameter). Fuconazole (100 g/mL in clean, distilled water) was used as the standard medication, while 10% DMSO served as the control. To hasten the dissipation process, 140 microliters from each of the test stock solutions of the compounds (100 and 200 g/mL in 10% DMSO) were added to these wells. The plates were then left to stand for an hour. After the 48-hour inoculation period at 37°C, the diameter of the zone of inhibition surrounding the wells was calculated using vernier calipers [9,10].

2.6. Antioxidant activity.

Using the DPPH approach, the antioxidant activity of the produced metal-based NP and NC was evaluated in accordance with the literature [11,12]. The substance was mixed with methanol in different concentrations before being poured into 5 mL vials. 3 mL of 0.004% DPPH in methanol was added to these test vials, and the solutions were then incubated for 30 min at room temperature in the dark. The standard was thought to be ascorbic acid. If DPPH removes hydrogen radicals from an external source, the absorption falls off stoichiometrically depending on how many electrons or hydrogen atoms are present overall. The DPPH

scavenging activity is computed using the following equation, and the absorbance was calculated to be 517 nm. The data collected are discussed in Table 3 accordingly.

Scavenging ratio (%) = [(Ai–Ao)/(Ac–Ao)] × 100%

where, Ai represents the absorbance while the existence of check material; Ao represents the amount of absorbance of a blank in the absence of a check material. Ac refers to the absorbance without the test material.

2.7. Antihemolytic activity.

The heparinized human red blood cells (according to the guidance of a medical counselor from Medical College, Mysore) were obtained, washed with saline (0.9%), and then centrifuged at 3000 rpm for 10 min to remove plasma. Exactly 40% v/v suspension was made with isotonic phosphate buffer at pH 7.4, and it was used as an RBC stock solution for further hemolytic assay. The Hemolysis assay was followed as per previous studies [13,14]. In the reaction mixture, 10% erythrocytes hemolysis was induced by an equal volume of 0.2 M AAPH containing extracts at different concentrations (0-100 µg/mL), without extract serves as negative control and normal erythrocytes, i.e., without AAPH or extracts serves as a positive control. Similarly, 0.2% Triton (in PBS) is taken for 100% hemolysis as a reference control. The reaction mixture was incubated for 2 h at 37°C and, at the end of incubation, diluted with 8 volumes of PBS and centrifuged at 2000 rpm for 10 min. supernatant was collected, and absorbance was read at 540 nm; the percentage of hemolysis was calculated, and results were expressed in IC_{50} value in comparison with L-ascorbic acid as standard.

3. Results and Discussion

3.1. Surface characterization of the adsorbent.

Surface characterization of CuO-ZnO done through SEM showed a moderate porous structure (Figure 2). When the Malachite green dye was absorbed, several pores became entirely filled with the adsorbate, producing a thin layer over the particle. IR spectra of CuO-ZnO showcased broadband between 3200-3500 cm^{-1}. The IR spectrum of CuO-ZnO is accredited to the presence of the hydroxyl group and an adsorbed water molecule (Figure 3).

A Keen edge band at 2932 cm^{-1} is due to the C-H stretching, and a band at 1466 cm^{-1} is due to C-O stretching [15]. Further, the bands at 1434, 1190, 1102, 1087, and 620 cm^{-1} are attributed to the C-O-C stretching. After adsorption of Malachite green dye on CuO -ZnO, it has been noted in the IR spectrum that the broad bands between 3100- 3500 cm^{-1} were due to stretching of $-NH_2$ group in Malachite green dye and between 3435-2989 cm^{-1} due to the hydroxyl group of CuO-ZnO has been vanished, which confirms the formation of hydrogen bonds between $-NH_2$ and hydroxyl groups. In addition, the disappearance of a strong peak at 1501 cm^{-1} for N-H Stretching confirms the strong adsorption of malachite green dye on CuO -ZnO. Finally, based on the absence of IR absorption frequencies, it attributes that the Malachite green dye has adsorbed on CuO-ZnO. The determination of the point of zero charge at the intersection of two plots (Figure 4) confirms that at pH 8 the adsorbent surface has zero charge [16].

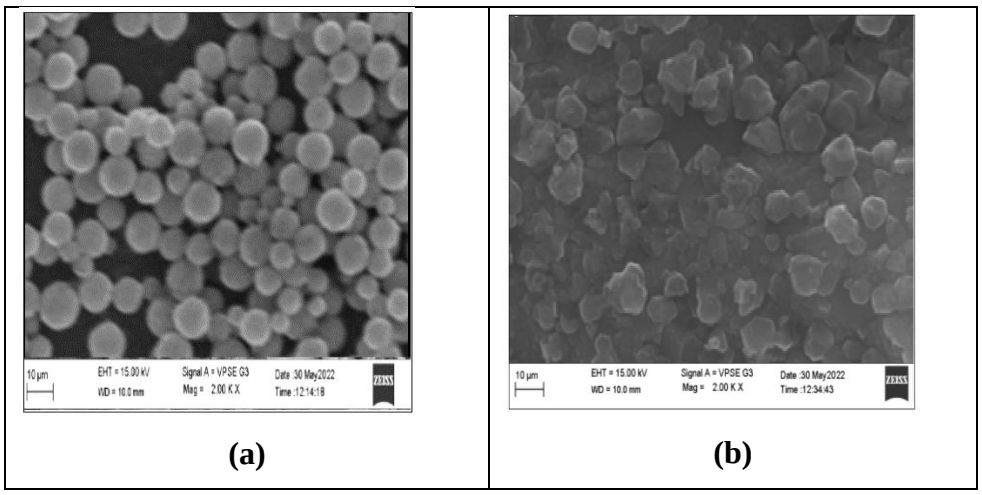

Figure 2. SEM images of (a) ZnO (b) Malachite green dye adsorbed CuO-ZnO.

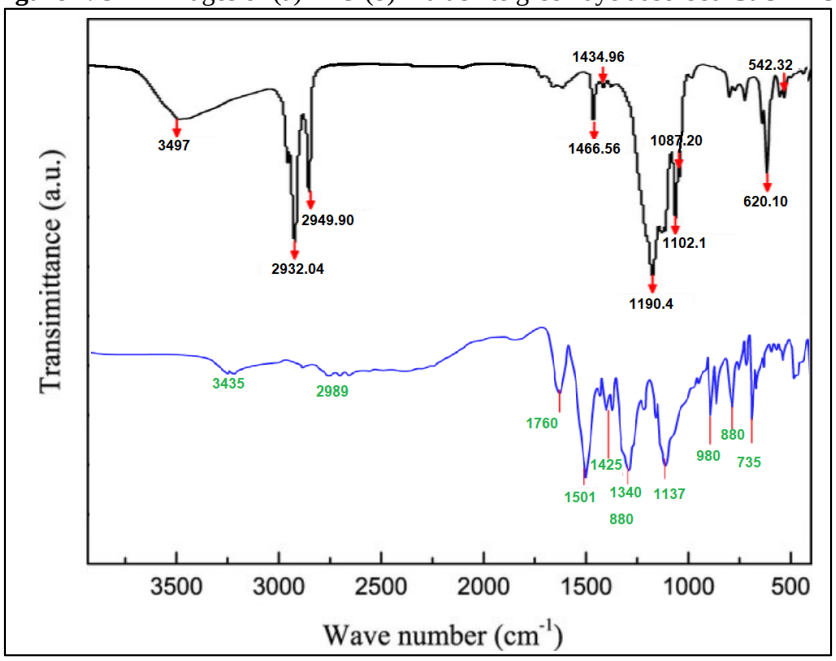

Figure 3. FTIR spectra of ZnO (black line), Malachite green dye adsorbed on CuO-ZnO (Blue line).

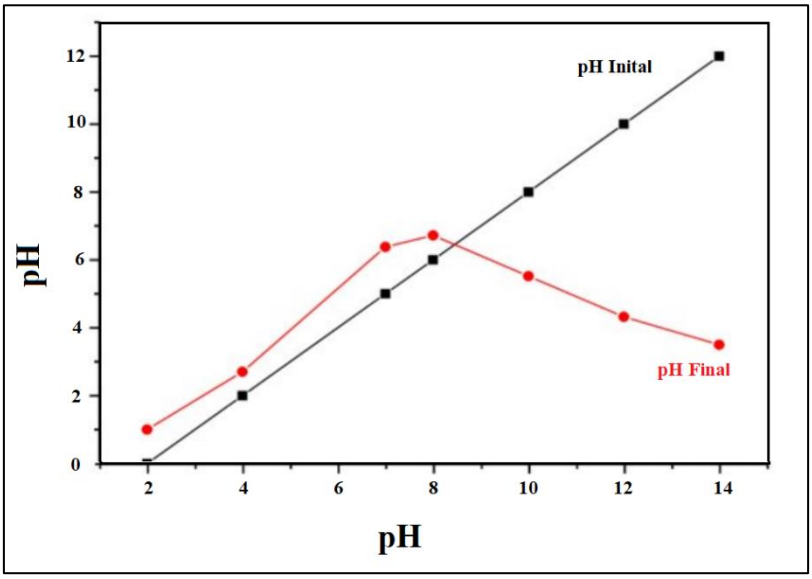

Figure 4. Zero Point charge of CuO –ZnO.

3.2. Batch adsorption studies.

3.2.1. Effect of pH and initial dye concentration.

It is paramount to ascertain the optimal status of each parameter to get maximum adsorption. Among these, pH is the vital parameter for the adsorption process since it influences the adsorption capacity via the adsorbent surface characteristics and the ionic forms of dye in the solution [17]. The maximum Malachite green dye removal by CuO -ZnO was at pH 8.0 (qe= 94.00 mg/g) with an initial concentration of 100 mg/L (Figure 5). The qe value increases with an increase in initial dye concentration from the range of 25-100 mg/L, as shown in Figure 6. The % qe value increased with a decrease in concentration and reached a maximum in the range of 150-250 mg/L concentration solution. Thereafter, the % qe value increases in concentration reaches to 70%.

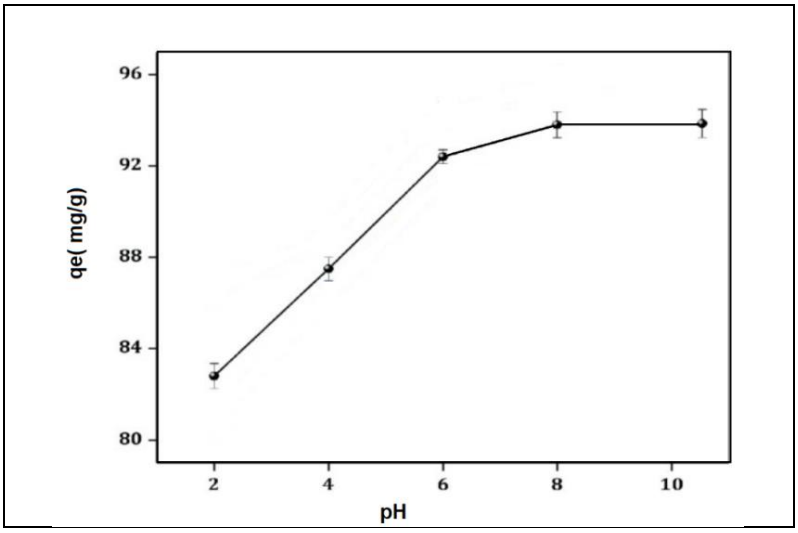

Figure 5. Effect of pH on adsorption of Malachite green dye.

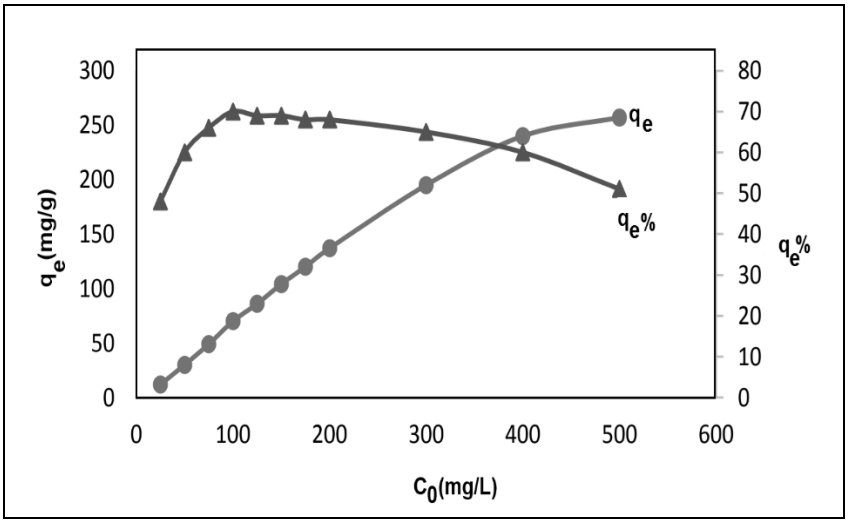

Figure 6. Effect of initial dye concentration on adsorption of Malachite green dye with qe%.

3.2.2. Effect of adsorbent dosage.

Adsorbent dose significantly influences the adsorption process since it determines the adsorption capacity for the adsorbate's initial concentration at the operating conditions. The effect of adsorbent dosage on Malachite green dye adsorption was investigated in the range of 0.200-3.000 g. It was observed that the percent Malachite green dye removal increased with a

decrease in adsorbent dose. The migration of Malachite green dye onto CuO -ZnO improved with a higher adsorbent dose. Any additional depletion in the adsorbent dosage after the limit had no substantial effect on adsorbate yield. This is due to almost all dye molecules binding onto the adsorbent surface and reaching equilibrium between dye molecules onto the adsorbent and in the solution [18]. The results are depicted in Figure 7.

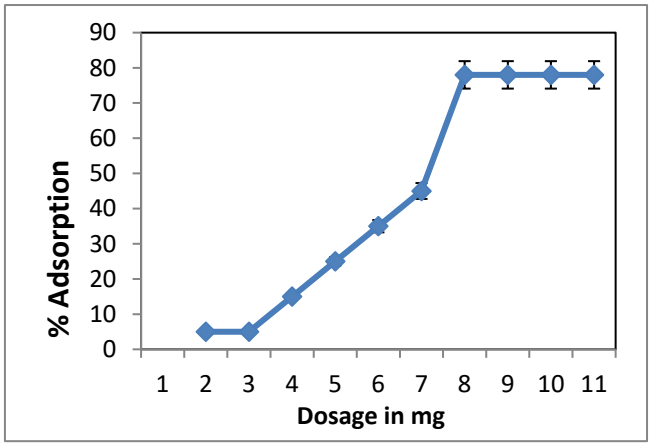

Figure 7. Effect of adsorbent dosage on adsorption of dye.

3.2.3. Effect of contact time on dye adsorption.

The effect of contact time and the adsorption of Malachite green dye onto CuO -ZnO was allowed to take place for 15, 30, 45, 60, 90, 120, 150, and 180 minutes in the initial 15 min it showed rapid adsorption to the extent of 60% of adsorption taking place, but as the contact time increased was further there was a slow increase in adsorption until 60 min then gradually it reached equilibrium as shown in Figure8. Aggregation of dye molecules causes them to diffuse deeper and with more energy into adsorbent structures as contact duration increases. Once the mesopores fill up and offer resistance to the diffusion of aggregated dye molecules in adsorbents, this aggregation negates the effect of contact time. [19].

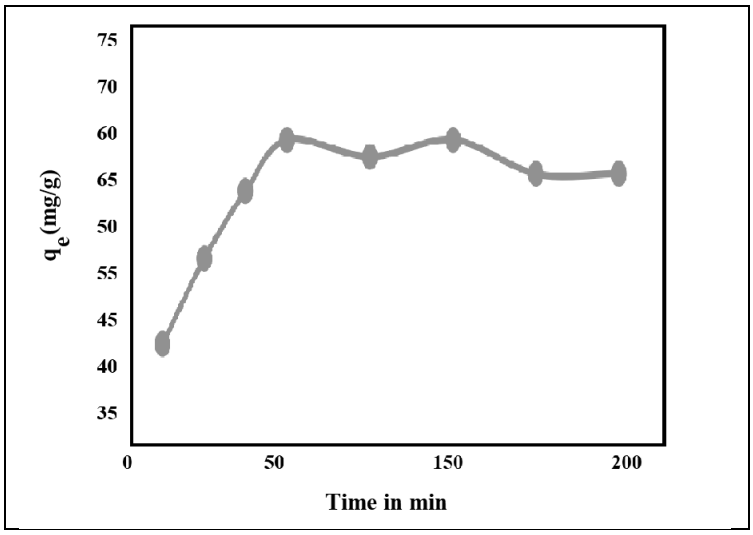

Figure 8. Effect of contact time on adsorption of dye.

3.2.4. Effect of temperature.

An additional aspect that affects the adsorption process is temperature. Adsorption studies were carried out at 30–5000 °C with three different dye concentrations, and the results

are shown in Figure 9. It was found that as the temperature rose, the adsorption capacity decreased, showing the endothermic nature of the process. The intra-particle diffusion phenomena, the mobility of the dye molecule and the lowering of kinetic energy, may be the causes of the improved adsorption with temperature [20].

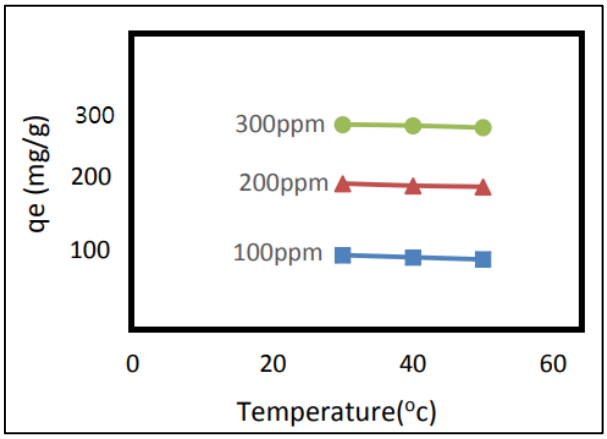

Figure 9. Effect of temperature on adsorption of dye.

3.3. Biological studies.

3.3.1. Antimicrobial activity.

Worldwide mortality was caused by the pathogenic pathogens' ongoing rise in resistance. Microbes have the genetic potential to develop resistance to therapeutically active medicines. Hence, efforts are often made to develop metal oxide nanoparticles with more antibacterial efficacy and lower toxicity. Also, several studies support the antibacterial effectiveness of nanoparticles and nanocomposites [21, 22]. In the existing study, the antimicrobial activities were performed for both metal oxide nanoparticles and nanocomposites, and it was evident that the CuO-ZnO NPs displayed superior antimicrobial activity compared to the CuO and ZnO NPs.

Table 2. Antimicrobial activity of metal oxides NPs and NC inhibition zone in mm.

Compound	Antibacterial activity								Antifungal activity			
	E.coli		*S.typhi*		*S.aureus*		*B.subtilis*		*A.niger*		*C. albicans*	
	100	200	100	200	100	200	100	200	100	200	100	200
CuO	26±0.49	28±1.06	25±0.50	27±1.33	24±0.55	26±0.60	25±1.19	27±1.12	21±0.54	23±1.11	22±0.47	24±0.37
ZnO	19±1.30	21±1.10	20±0.69	22±0.42	21±0.54	23±1.25	18±1.42	20±0.53	15±0.89	17±1.55	18±1.17	19±1.56
CuO-ZnO	30±1.11	32±1.14	31±0.49	33±0.51	32±1.21	34±0.43	29±1.19	31±1.25	28±1.13	30±1.62	26±1.19	27±1.22
Std 1	40±0.66	42±0.51	39±0.71	41±1.41	42±0.68	44±0.44	40±1.29	43±1.58	-	-	-	-
Std 2	-	-	-	-	-	-	-	-	35±0.68	37±0.59	36±1.20	38±0.72

*Std 1: Chloramphenicol, Std 2: Fluconazole
*Each value is expressed as mean ± SD of three replicates for the zone of inhibition.

The values have been tabulated in Table 1 and depicted in Figures 10(a) and (b). Generally, nano size renders more surface area, which facilitates high adsorption. Hence, when NPs enter a cell by adsorption, the enzyme activity is damaged, which then affects physiological functions like protein synthesis and DNA replication before preventing the

growth of microorganisms. The impressive antibacterial effectiveness of the NPs also explains why they have a greater surface charge density, which increases their attraction for negatively charged microbial cell membranes and inhibits the multiplication of those cells [23].

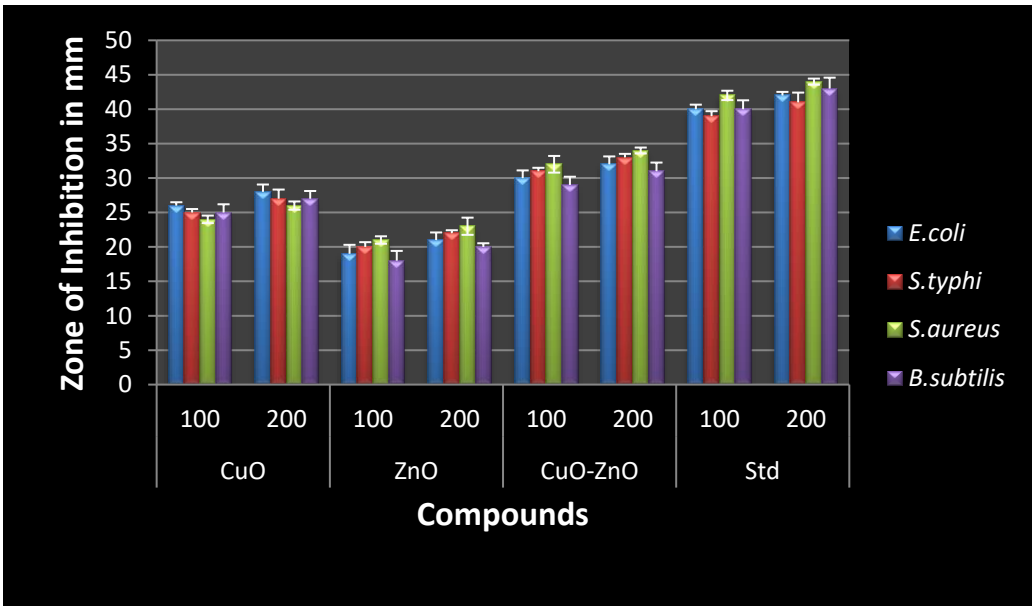

Figure 10. (a) Antibacterial activity of Metal oxide NPs and NC.

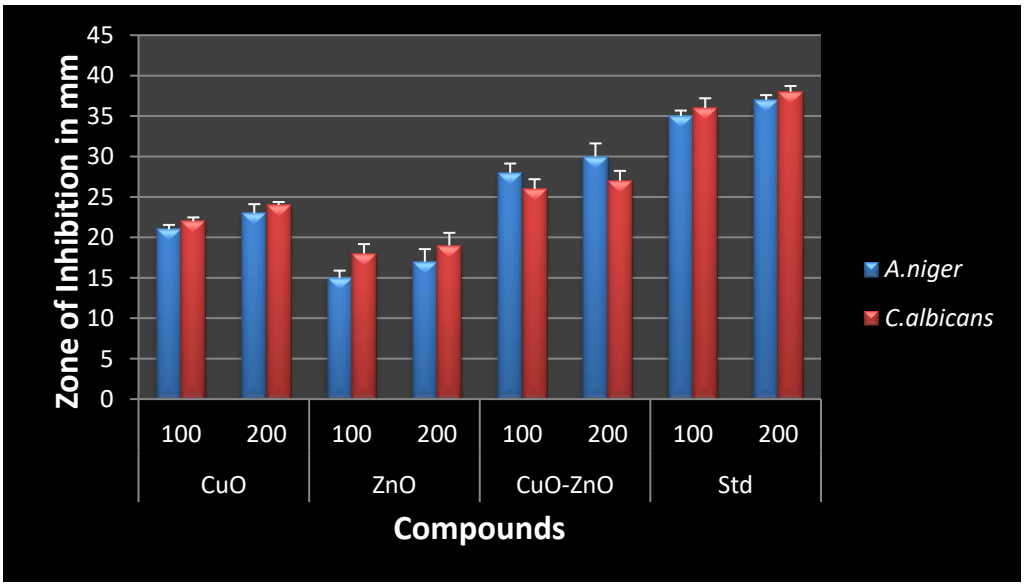

Figure 10. (b) Antifungal activity of Metal oxide NPs and NC.

3.3.2. Antioxidant activity.

One of the crucial fundamental investigations in nanoscience and nanotechnology is evaluating the antioxidant activity of nanomaterials. Therefore, the DPPH assay, which is thought to be the most accurate method, was used to assess the antioxidant capacity of synthetic metal oxide NPs. In general, a material's capacity to donate an active hydrogen atom or transfer electrons is connected to that material's antioxidant activity. By accepting an electron or hydrogen from antioxidant species in the experiment, the DPPH radical is reduced, resulting in a bright yellow tint and a significant decrease in the maximum absorbance [24].

The current study investigated the percentage radical scavenging activity of synthesized metal oxide NPs and NC at different concentrations (20, 40, 60, 80, and 100 µg/mL). It was noted that the percentage of scavenging activity of synthesized Nps and NCs was increased

upon enhancing the concentration. Of all the synthesized compounds, CuO -ZnO NPs demonstrated the highest antioxidant capability but were lesser than the standard. The recorded data has been placed in Table 3 and graphed in Figure 11. The antioxidant activity of metal oxide nanoparticles may be attributed to the transfer of electrons located on the oxygen atom to the odd electron located at the nitrogen atom in DPPH, thereby causing a decrease in absorbance at 517 nm.

Table 3. Antioxidant activity of metal oxides NPs and NC.

Compounds	% of Scavenging activity (concentrations in µg/mL)				
	20	40	60	80	100
CuO	42.31±0.44	48.11±0.59	55.22±1.06	61.87±0.69	64.36±1.22
ZnO	38.27±0.41	44.30±0.18	50.63±0.37	54.08±0.40	59.15±0.35
CuO -ZnO	46.18±0.83	57.05±1.23	63.49±0.64	65.70±0.67	73.75±1.39
Std	59.04±0.69	65.38±1.15	71.43±0.82	79.13±0.55	82.52±1.45

*Std:Butylatedhydroxytoluene
*Each value is expressed as mean ± SD of three replicates for the zone of inhibition.

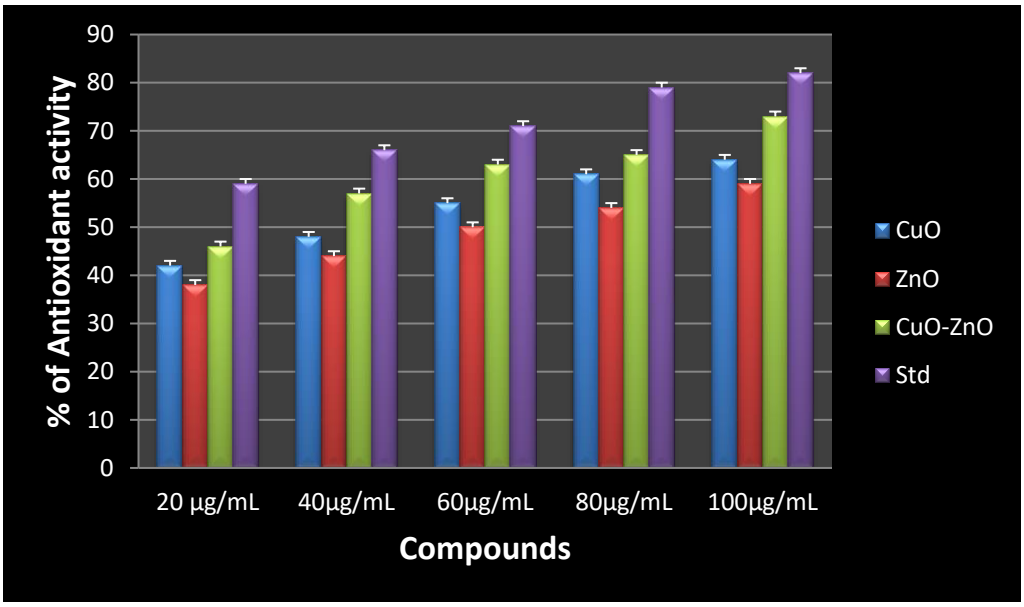

Figure 11. Antioxidant activity of Metal oxide NPs and NC.

3.3.3. Antihemolytic Activity.

Hemolysis is the term used to describe the breakdown of red blood cells (RBC) and the release of hemoglobin into the plasma. This study examined whether metal oxide nanoparticles may shield red blood cells from the oxidative harm caused by AAPH-induced hemolysis.

Table 4. The antihemolytic activity of metal oxides NPs and NC.

Compounds	IC_{50} (µg/mL)
CuO	27.43±0.66
ZnO	34.13±0.54
CuO -ZnO	24.08±0.78
Std	12.23±0.69

*Std : Vit-C

Table 4 summarizes the anti-hemolytic activity of the tested compounds in terms of IC50 values, Figure 12(a) graphs the activity results, and Figure 12(b) showcases the

protective effect exerted by metal oxide NPs on red blood cell damage induced by AAPH. From the obtained results, it was observed that ZnO/CuO provided the maximum protective effect against AAPH-induced oxidative hemolysis with an IC50 value of (24.08 µg/mL) while CuO NP had an observable protective effect with an IC50 value of (27.43 µg/mL). Overall, all the prepared metal oxide NPs and nanocomposites appeared to have anti-hemolytic properties to some extent but were not as effective as the standard.

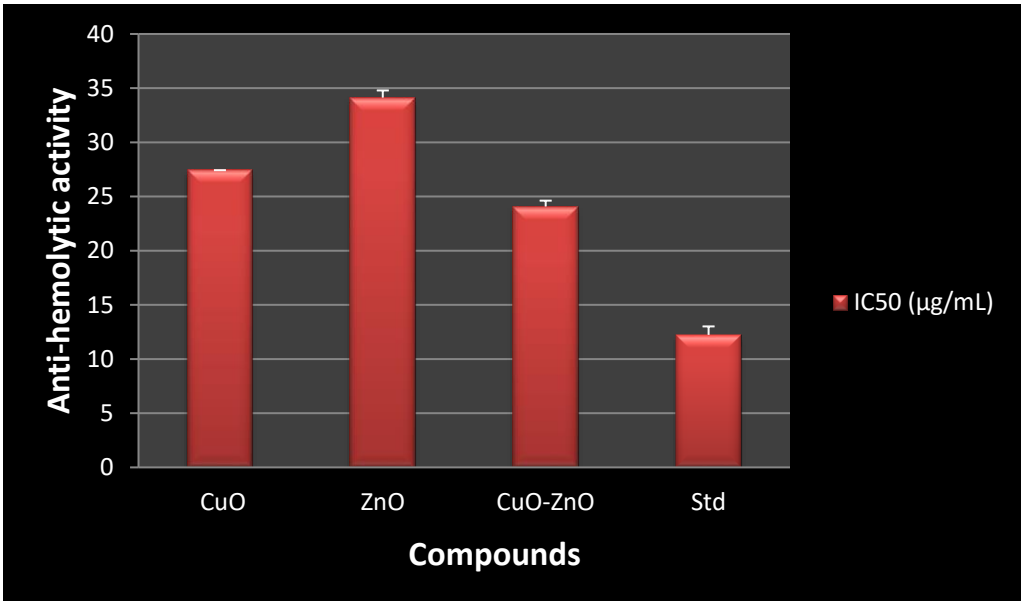

Figure 12. (a) Anti-hemolytic assay of metal oxides NPs and NC.

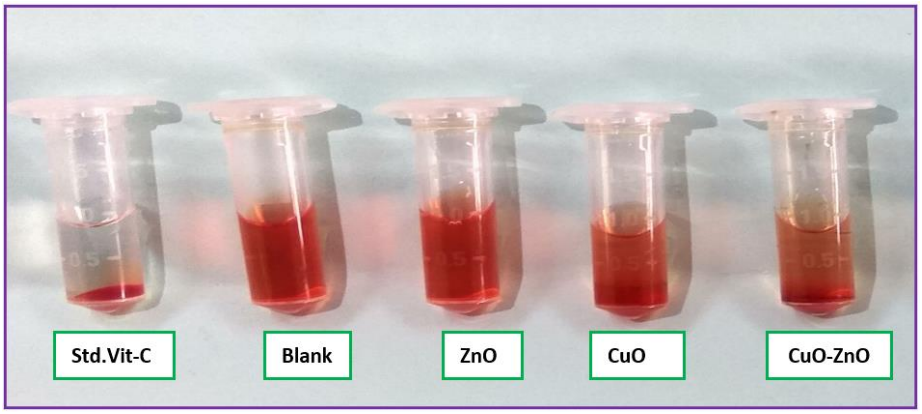

Figure 12. (b) Protective effect exerted by metal oxides NPs and NC on red blood cell damage induced by AAPH.

4. Conclusions

The existing study features CuO-ZnO, which has been prepared and assessed via different techniques that strongly validated the efficient dye adsorption of MG dye from the water waste and confirmed the precipitation method's efficacy. Studies of the structure of the CuO-ZnO were cautiously carried out in detail by diverse analytical procedures. The general data support the proposed structure and recommend that the synthesized CuO-ZnO has a spherical shape. The physicochemical process of the dosage was adsorbed at 0.1g with 70% of q_e. Upon biological screening, the NC demonstrated profound activities compared to the NP. Furthermore, we can consider that the synthetic CuO-ZnO materials have promising eco-friendly capabilities for the quantitative sorption of dye-polluted wastewater.

Funding

This research received no external funding.

Acknowledgments

The authors thank the Directorate of Minorities, Bangalore, Karnataka, India, for their financial support. They are also grateful to the Principal, JNN College of Engineering, and the Principal, of Sahyadri Science College, Shimoga, for supporting this research work. A special thanks go to the Centralized Instrumentation Facility, Mysore University, and SAIF, Karnataka University Dharwad, for rendering analytical as well as spectral data. We also appreciate Cheliyan Bio-tech, Mysore, Karnataka, India, for providing results on biological activities.

Conflicts of Interest

The authors declare no conflict of interest.

References

1. Velempini, T.; Prabakaran, E.; Pillay, K. Recent developments in the use of metal oxides for photocatalytic degradation of pharmaceutical pollutants in water-A review. *Materials Today Chemistry* **2021,** *19*, 100380, https://doi.org/10.1016/j.mtchem.2020.100380.
2. Liu, J.; Luo, Z.; Mao, X.; Dong, Y.; Peng, L.; Sun-Waterhouse, D.; Kennedy, J.V.; Waterhouse, G.I.; Recent Advances in Self-Supported Semiconductor Heterojunction Nanoarrays as Efficient Photoanodes for Photoelectrochemical Water Splitting. *Nano micro Small* **2022,** *18*, 2204553, https://doi.org/10.1002/smll.202204553.
3. Lu, X.; Hart, J.N.; Yao, Y.; Toe, C.Y.; Scott, J; N, Y.H. Cu_2O photocatalyst: Activity enhancement driven by concave surface. *Materials Today Energy* **2020,** *16*, 100422, https://doi.org/10.1016/j.mtener.2020.100422.
4. Li, Z.; Chai, F.; Yang, C.; Yang, L. Co-precipitation mechanism of nanoscale particles and mechanical properties in multicomponent ultra-high strength low carbon steel. *Materials Science and Engineering: A* **2019,** *748*, 128-136, http://dx.doi.org/10.1016/j.msea.2019.01.086.
5. Islam, M.R.; Obaid, J.E.; Saiduzzaman, M.; Nishat, S.S.; Debnath, T.; Kabir, A. Effect of Al doping on the structural and optical properties of CuO nanoparticles prepared by solution combustion method: Experiment and DFT investigation. *Journal of Physics and Chemistry of Solids* **2020**, *147*, 109646, https://doi.org/10.1016/j.jpcs.2020.109646.
6. Jinendra, U.; Kumar, J.; Nagabhushana, B.M.; Raghu, A.V.; Bilehal, D. Facile synthesis of CoFe2O4 nanoparticles and application in removal of malachite green dye. *Green Materials*, **2019,** *7*, 137-142, https://doi.org/10.1680/jgrma.18.00054.
7. Shah, M.Z.U.; Sajjad, M.; Hou, H.; Rahman, S.; Mahmood, A.; Aziz, U. ; Shah, A. A new CuO/TiO2 nanocomposite: An emerging and high energy efficient electrode material for aqueous asymmetric supercapacitors. *Journal of Energy Storage* **2022**, *55*, 105492, https://doi.org/10.1016/j.est.2022.105492.
8. Ramesh, G.; Daravath, S.; Swathi, M.; Sumalatha, V; Shankar, D.S. Investigation on Co (II), Ni (II), Cu (II) and Zn (II) complexes derived from quadridentate salen-type Schiff base: structural characterization, DNA interactions, antioxidant proficiency and biological evaluation. *Chemical Data Collections*, **2020,** *28*, 100434, https://doi.org/10.1016/j.cdc.2020.100434.
9. Lubna, A.; Moinuddin, K.M.H.; Vagdevi, H.M.; Malathesh, P.; Mohammed, S.R.; Mussuvir P.K.M. Investigation on Co(II), Ni(II), Cu(II), and Zn(II) complexes derived from novel *N′*-(3-hydroxybenzoyl)thiophene-2-carbohydrazide: structural characterization, electrochemical detection of biomolecules, molecular docking, and biological evaluation. *Emergent Materials* **2021,** *23*, https://doi.org/10.1007/s42247-021-00312-4.
10. Vittal Rao, K.S.; Malathesh, P.; Lubna, A.; Pampa, K.J. Synthesis, spectral characterization, electrochemical studies of pesticide and biological evaluation of transition metal complexes of azo dye derived from substituted phenyl pyrazole. *Journal of the Indian Chemical Society* **2022,** *99*, 100788, https://doi.org/10.1016/j.jics.2022.100788.

11. Ranjitha, N.; Krishnamurthy, G.; Bhojya Naik, H.S.; Malathesh, P.; Lubna, A.; Sumadevi, K.R.; Manjunatha, M.N. Structural elucidation, voltammetric detection of dopamine, molecular docking and biological inspection of novel 4-aminoantipyrine derived Schiff bases in Co (II), Ni (II) and Cu (II) complexes. *Inorganica Chimica Acta* **2022,** *543*, 121191. https://doi.org/10.1016/j.ica.2022.121191.
12. Kumar, N.S.; Krishnamurthy, G.; Pari, M.; Naik, T.R.; Kumara, K.J.; Naik, S.; Kandagalla, S.; Naik, N. Synthesis, characterization, electrochemistry, biological and molecular docking studies of the novel Co (II), Ni (II) and Cu(II) complexes derived from methanethiol bridged (2-((1H-benzo [d] imidazol-2-yl) methylthio)-1H-benzo [d] imidazol-6-yl)(phenyl) methanone. *Journal of Molecular Structure* **2020,** *1220*, 128586, https://doi.org/10.1016/j.molstruc.2020.128586.
13. Lakshmegowda, S.B.; Rajesh, S.K.; Kandikattu, H.K.; Nallamuthu, I.; Khanum, F. In Vitro and In Vivo Studies on Hexane Fraction of Nitzschia palea, a Freshwater Diatom for Oxidative Damage Protective and Anti-inflammatory Response. *RevistaBrasileira de Farmacognosia* **2020**, *30*, 189-201, http://dx.doi.org/10.1007/s43450-020-00008-6.
14. Sudarshan, B.L.; Maheshwar, P.K.; Priya, P.S.; Sanjay, K.R. Volatile and phenolic compounds in freshwater diatom Nitzschia palea as a potential oxidative damage protective and anti-inflammatory source. *Pharmacognosy Magazine* **2019**, *15*, 228, http://dx.doi.org/10.4103/pm.pm_649_18.
15. Madhan, G.; Begam, A.A.; Varsha, L.V.; Ranjithkumar, R.; Bharathi, D. Facile synthesis and characterization of chitosan/zinc oxide nanocomposite for enhanced antibacterial and photocatalytic activity. *International Journal of Biological Macromolecules* **2021**, *190*, 259-269, https://doi.org/10.1016/j.ijbiomac.2021.08.100.
16. Khalaji, A.D.; Pazhand, Z.; Kiani, K. CuO nanoparticles: preparation, characterization, optical properties, and antibacterial activities. *J Mater Sci: Mater Electron* **2020**, *31*, 11949–11954, https://doi.org/10.1007/s10854-020-03749-1.
17. Abdullah, M.A.; Ibrahim, H.A.; Abdullah, A.A.; Ayoub, A.A.; ZakiEldin, A.A.; Ebraheem Abdu, M.S. Adsorptive performance of aminoterephthalic acid modified oxidized activated carbon for malachite green dye: mechanism, kinetic and thermodynamic studies. *Separation Science and Technology* **2021,** *5*, 835-846, https://doi.org/10.1080/01496395.2020.1737121.
18. Zhang, W.; Zhu, N.; Ding, L.; Hu, Y.; Wu, Z. Efficacious CO2 Adsorption and Activation on Ag Nanoparticles/CuO Mesoporous Nanosheets Heterostructure for CO_2 Electroreduction to CO. *Inorganic Chemistry*, **2021**, *60*, 19356-19364, https://doi.org/10.1021/acs.inorgchem.1c03183.
19. Kekkonen, J.M.; Mousapour, M.; Jokilaakso, A.; Lundström, M. The Oxidation of Copper in Air at Temperatures up to 100 C. *Corrosion and Materials Degradation* **2021,** *2*, 625-640, https://doi.org/10.3390/cmd2040033.
20. Saravanan, R.; Gupta, V.K.; Prakash, T.; Narayanan, V.; Stephen, A. Synthesis, characterization and photocatalytic activity of novel Hg doped ZnO nanorods prepared by thermal decomposition method. *Journal of Molecular Liquids* **2013,** *178*, 88-93, https://doi.org/10.1016/j.molliq.2012.11.012.
21. Bonini, C.; Chiummiento, L.; De Bonis, M.; Funicello, M.; Lupattelli, P.; Suanno, G.; Berti, F.; Campaner, P. Synthesis, biological activity and modelling studies of two novel anti HIV PR inhibitors with a thiophene containing hydroxyethylamino core. *Tetrahedron* **2005**, *61*, 6580-6589, https://doi.org/10.1016/j.tet.2005.04.048.
22. Beyene, A.M.; Moniruzzaman, M.; Karthikeyan, A.; Min T. Curcumin nanoformulations with metal oxide nanomaterials for biomedical applications. *Nanomaterials* **2021,** *2*, 460, https://doi.org/10.3390/nano11020460.
23. Kotrange, H.; Najda, A.; Bains, A.; Gruszecki, R.; Chawla P.; Tosif, M.M. Metal and metal oxide nanoparticle as a novel antibiotic carrier for the direct delivery of antibiotics. *International Journal of Molecular Sciences* **2021,** *17*, 9596, https://doi.org/10.3390/ijms22179596.
24. Asiri, Y.I.; Muhsinah, A.B.; Alsayari, A.; Venkatesan, K.; Al-Ghorbani, M.; Mabkhot, Y.N. Design, synthesis and antimicrobial activity of novel 2-aminothiophene containing cyclic and heterocyclic moieties. *Bioorganic & Medicinal Chemistry Letters* **2021**, *44*, 128117, https://doi.org/10.1016/j.bmcl.2021.128117.